Supplementary Information

Skillful Seasonal Predictions of Continental East-Asian Summer Rainfall by Integrating its Spatio-Temporal Evolution

Jieru Ma[1], Hong-Li Ren[1,*], Ming Cai[2], Yi Deng[3], Chenguang Zhou[1],
Jian Li[1], Huizheng Che[4], Lin Wang[5]

[1] State Key Laboratory of Severe Weather and Institute of Tibetan Plateau Meteorology, Chinese Academy of Meteorological Sciences, Beijing, China

[2] Department of Earth, Ocean, and Atmospheric Science, Florida State University, Tallahassee, FL, USA

[3] School of Earth and Atmospheric Sciences, Georgia Institute of Technology, Atlanta, GA, USA

[4] Key Laboratory of Atmospheric Chemistry of China Meteorological Administration, Chinese Academy of Meteorological Sciences, Beijing, China

[5] Institute of Artificial Intelligence for Meteorology, Chinese Academy of Meteorological Sciences, Beijing, China

Correspondence to: H.-L. Ren
renhl@cma.gov.cn

Contents of this file

Supplementary Table 1. Details of the nine dynamical models in the period of 1993–2016 used in this study. These nine dynamical models are provided by the China Meteorological Administration (CMA) and the Copernicus Climate Change Service (C3S).

Number	Full name of the model and reference	Abbreviation	Atmospheric horizontal resolution	Hindcast ensemble size
1	BCC-CSM1.1m from the China Meteorological Administration[1]	CMA	T106	24
2	SPS3.5 of Euro-Mediterranean Center on Climate Change (Centro Euro-Mediterraneo sui Cambiamenti Climatici)[2]	CMCC	0.5°×0.5°	40
3	Deutscher Wetterdienst GCFS2.0[3]	DWD	T127	30
4	GEM5-NEMO of Environment and Climate Change Canada[4]	ECCC	1°×1°	10
5	European Centre for Medium-Range Weather Forecasts SEAS5[5]	ECMWF	$T_{co}319$	25
6	Japan Meteorological Agency Coupled Prediction System version 3[6]	JMA	TL319	10
7	Météo-France System 8[7]	MF	TL359	25
8	CFSv2 of National Centers for Environmental Prediction[8]	NCEP	T126	24
9	The United Kingdom Met Office GloSea6[9]	UKMO	N216	28

Supplementary Table 2. The information of six climate indices and corresponding correlations with six precursors. Column 1 lists the six climate indices denoting climate variability modes influencing East Asia rainfall variability, and columns 3–8 represent the correlation coefficients between climate indices and precursors in this study. Endings with two (one) asterisks indicate the values exceeding the 99% (90%) confidence level.

Definition and Reference	Data Source	Abbreviation	Autumn IAP	Spring EIP	Winter EWP	Autumn ET	Winter ESAP	Spring EPT
Spatial mean of near-surface air temperature (SAT) over north Pacific Ocean (30 ° to 50 ° N, 140 ° E to 140°W)[10]	1	NPSST	-0.45**					
Snow depth anomalies in Tibetan Plateau (26° to 40°N, 73° to 105°E)[11]	2	TPSD	0.44**					0.48**
Spatial mean sea level pressure over Mascarene (25° to 35°S, 40° to 90°E)[10]	3	MSLP	-0.35*					
Meridional land-ocean SAT contrast between East Asia (20-60N, 60-120E) and south Indian Ocean (0° to 40°S, 50° to 110°E)[10]	1	MLOC		0.52**	-0.54**	-0.51**	0.57**	
Western Pacific subtropical high defined as U_{850} (25° to 35°N,120° to 150°E) minus U_{850} (10° to 20°N,130° to 150°E)[12]	4	WPSH				0.39**		
Sea surface temperature anomalies over eastern tropical Pacific ocean (5°S to 5°N, 150° to 90°W)[13]	5	Niño 3						0.96**

Supplementary Table 3. Details of three satellite-gauge-based precipitation datasets for the period of 1980–2022.

Number	Full name of the dataset and references	Abbreviation	Provider	Resolution	Uniform Resource Locator
1	Global Precipitation Climatology Project analysis product[14]	GPCP	NOAA Physical Sciences Laboratory (PSL)	2.5° × 2.5°	https://psl.noaa.gov/data/gridded/data.gpcp.html
2	Climate Prediction Center merged analysis of precipitation[15]	CMAP	NOAA PSL	2.5° × 2.5°	https://psl.noaa.gov/data/gridded/data.cmap.html
3	Global Precipitation Climatology Centre precipitation dataset[16]	GPCC	NOAA PSL	0.5° × 0.5°	https://psl.noaa.gov/data/gridded/data.gpcc.html

Supplementary Table 4. A list of data sources for the climate indices listed in Supplementary Table 2. The information includes the dataset name and the Uniform Resource Locator.

Number	Dataset name	Uniform Resource Locator
1	HadCRUT ensemble mean	https://www.metoffice.gov.uk/hadobs/hadcrut5/data/HadCRUT.5.0.2.0/download.html
2	Daily snow depth dataset	https://data.tpdc.ac.cn/en/data/df40346a-0202-4ed2-bb07-b65dfcda9368/
3	NCEP/NCAR reanalysis 2	https://downloads.psl.noaa.gov/Datasets/ncep.reanalysis2/Monthlies/surface/
4	NCEP/NCAR reanalysis 2	https://downloads.psl.noaa.gov/Datasets/ncep.reanalysis2/pressure/
5	Niño 3	https://psl.noaa.gov/data/correlation/nina3.anom.data

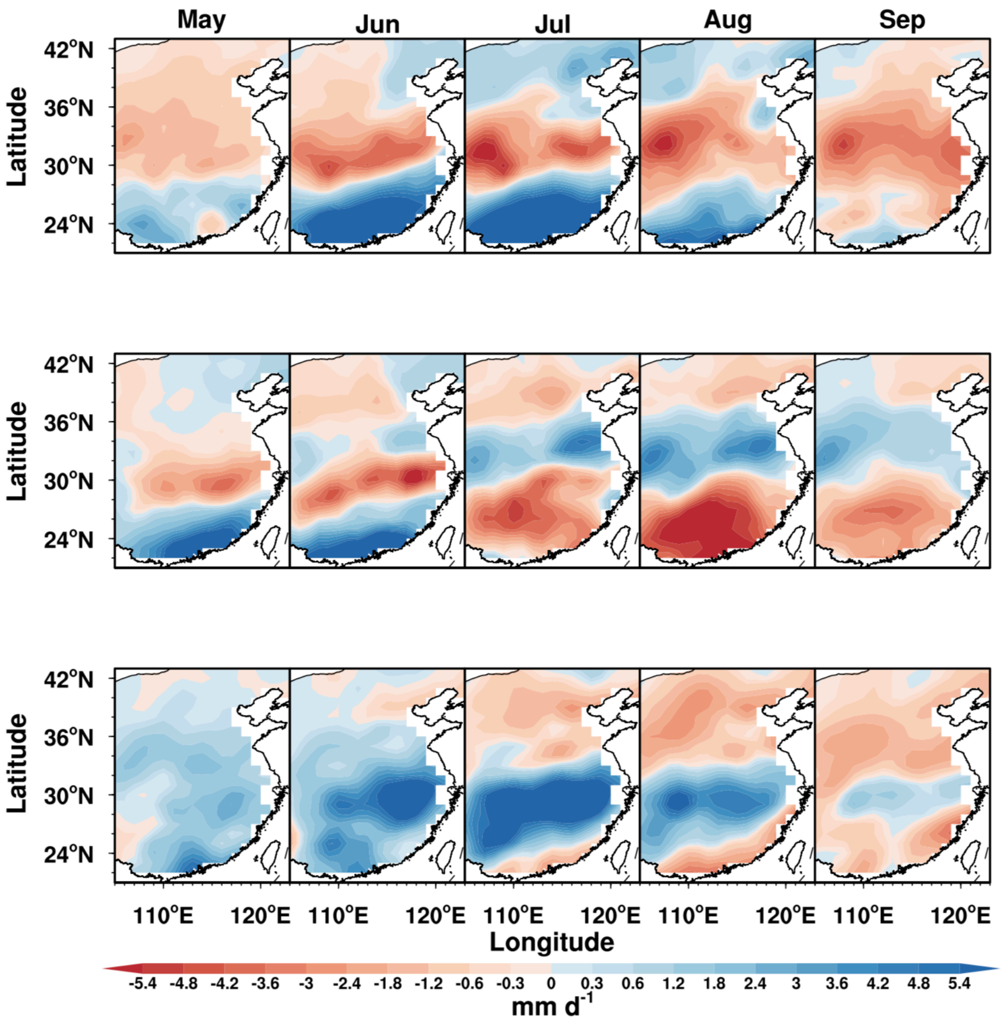

Supplementary Figure 1. The monthly rainfall patterns of the three spatiotemporal patterns of East-Asian rainfall anomalies in boreal summer. The three rows from top to bottom represent the monthly spatial patterns of the three distinct spatiotemporal patterns identified in the training period of 1980–2009. Unit of the color bar is mm d^{-1}. The five columns from left to right are spatial rainfall patterns for May, June, July, August, and September, respectively.

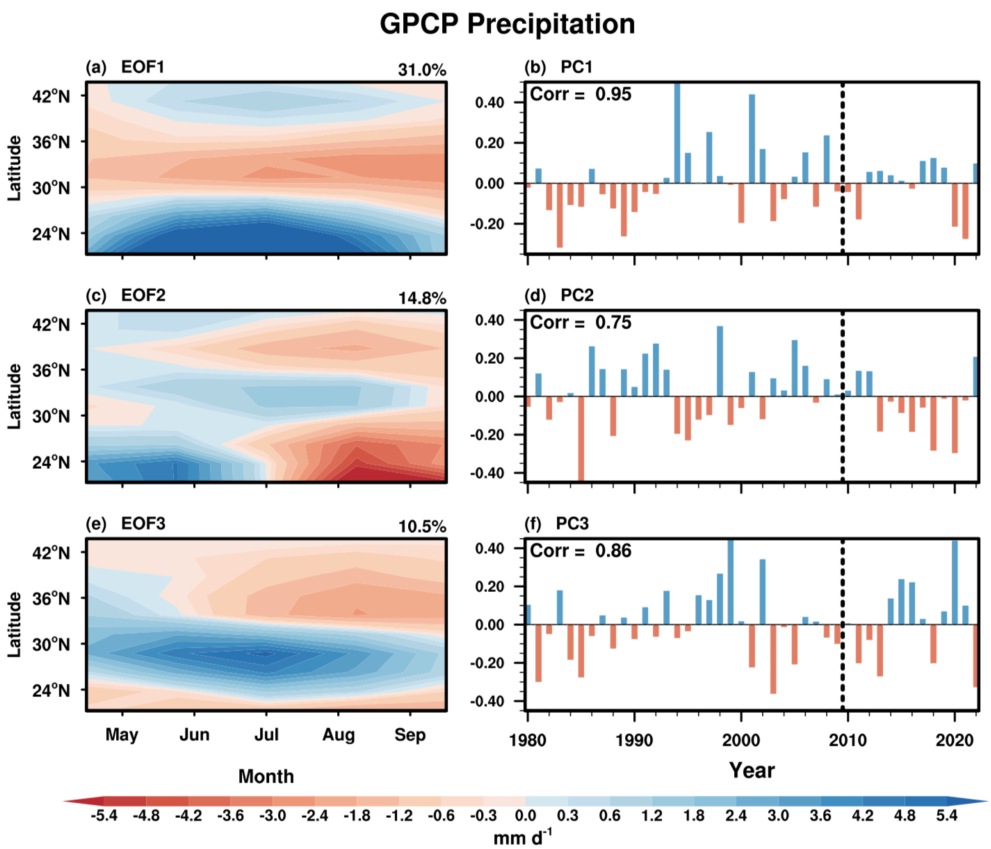

Supplementary Figure 2. Spatiotemporal patterns of continental East-Asian summer rainfall anomalies derived from GPCP observation. The left panels (a, c, e) display the spatiotemporal evolution patterns corresponding to the leading three modes of empirical orthogonal functions (EOFs) derived from monthly precipitation anomalies zonally averaged over East Asia during training period of boreal 1980–2009 summers. The unit of the color bar for the spatiotemporal patterns is mm d^{-1}. The bars in the right panels (b, d, f) are the year-to-year variability of normalized principal components (PCs) of the three spatiotemporal patterns.

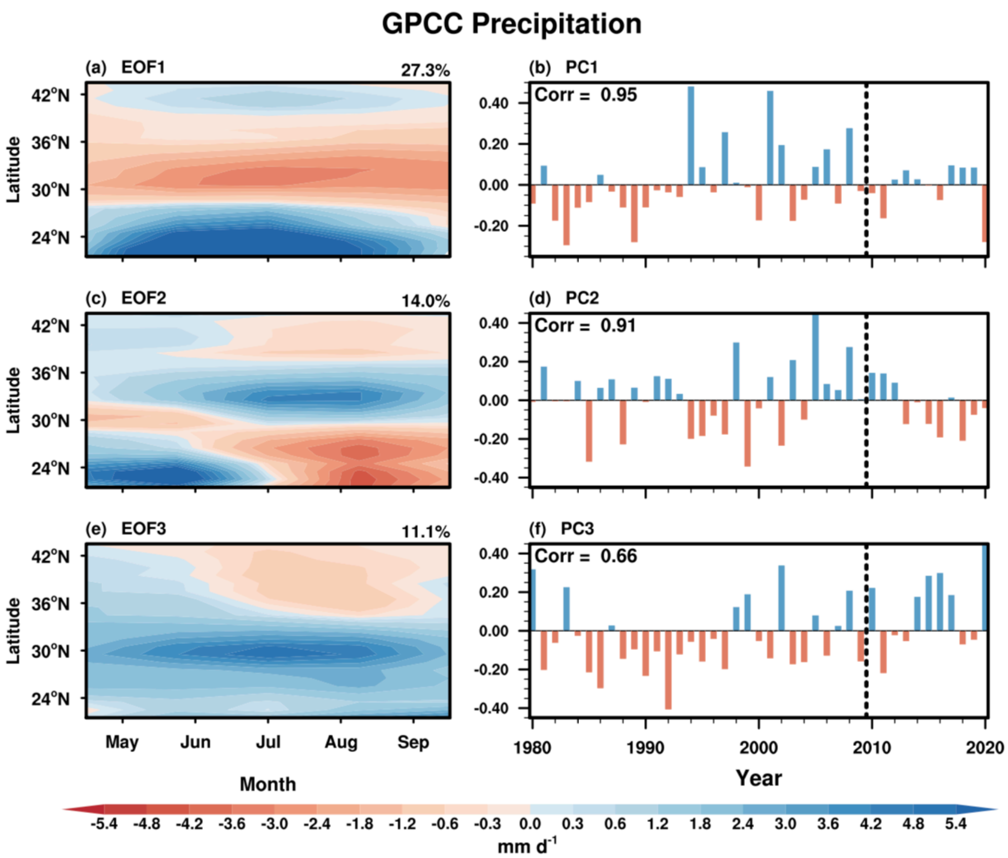

Supplementary Figure 3. Same as Supplementary Fig. 2, but for the GPCC.

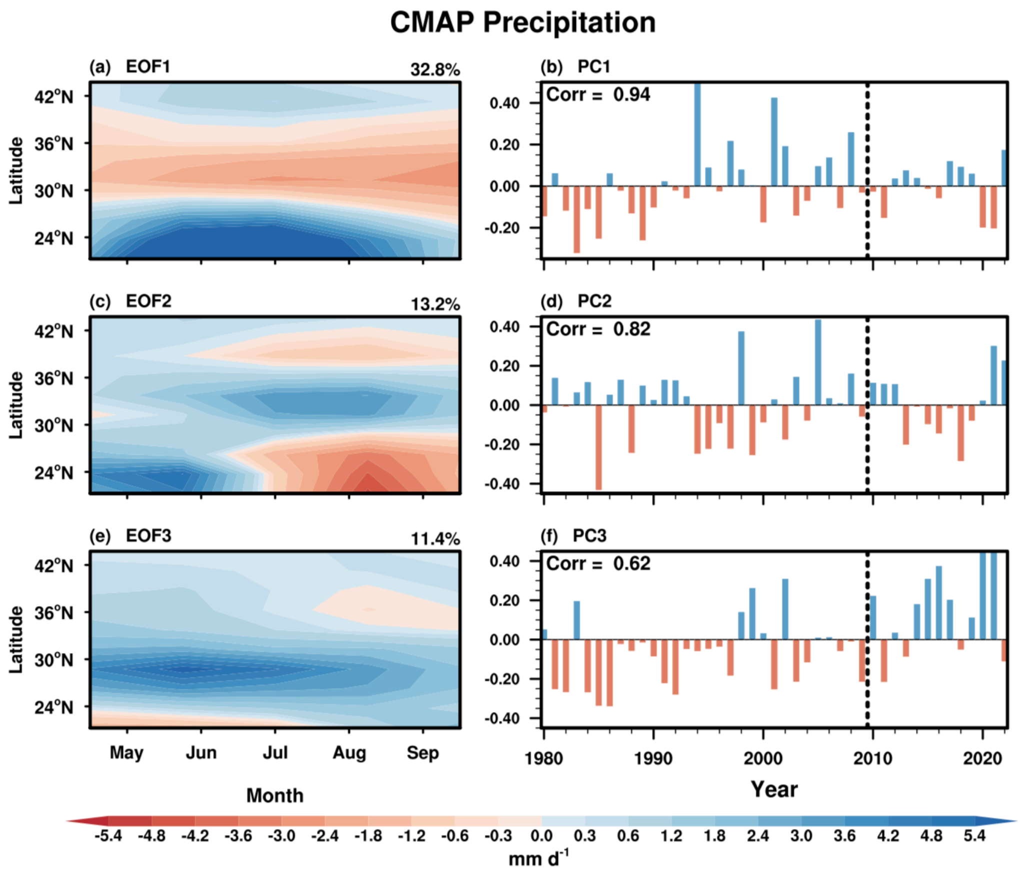

Supplementary Figure 4. Same as Supplementary Fig. 2, but for the CMAP.

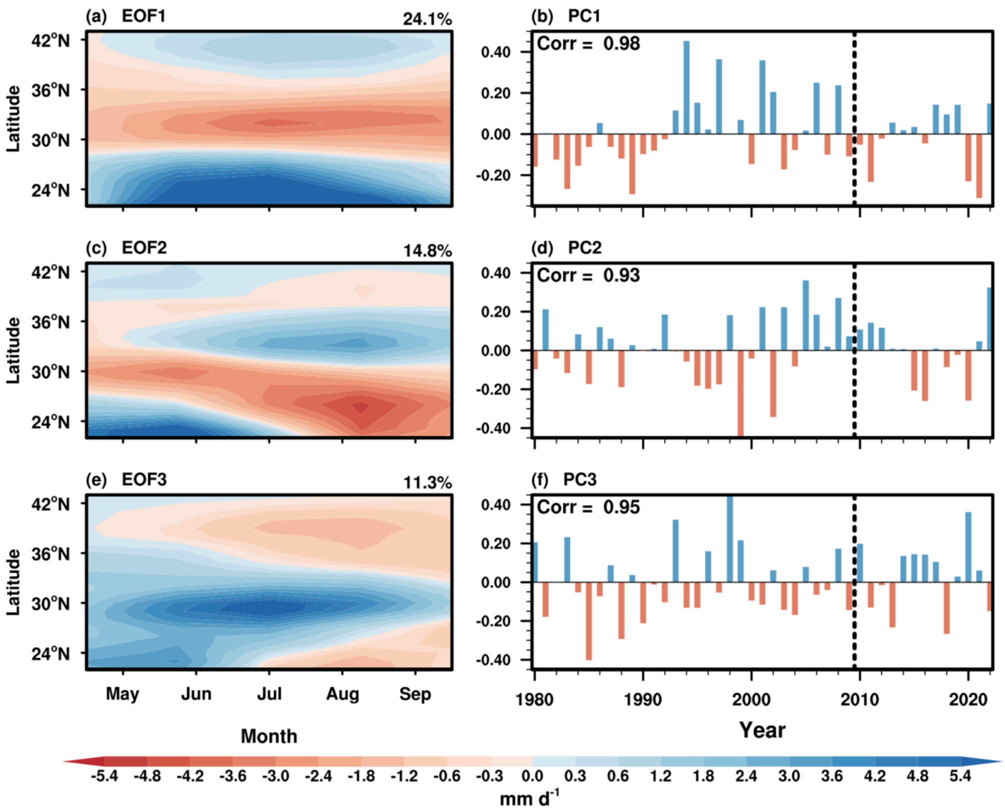

Supplementary Figure 5. Same as Supplementary Fig. 2, but for the monthly station-based precipitation.

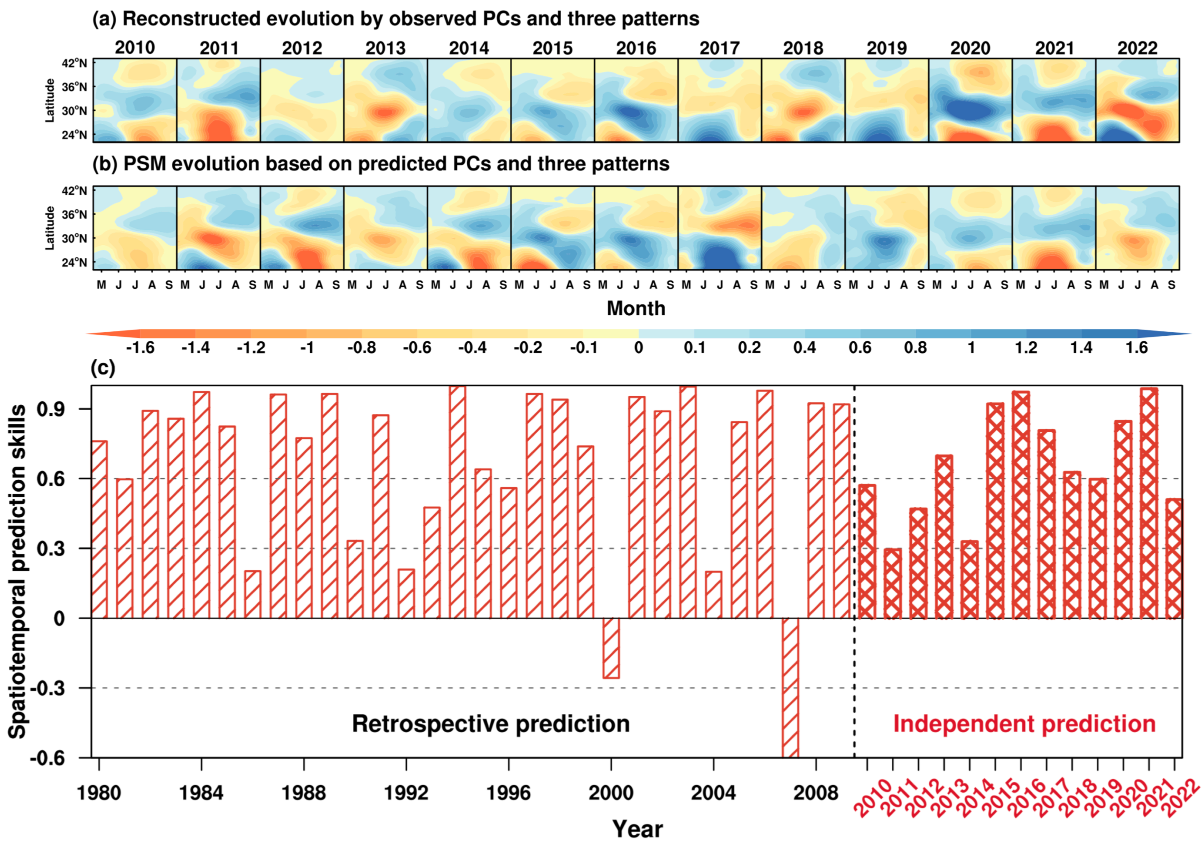

Supplementary Figure 6. Prediction skills of spatiotemporal evolution based on the three spatiotemporal patterns of East-Asian rainfall anomalies in the physical-statistical prediction model. (a) The observed spatiotemporal evolution using the three spatiotemporal patterns in the independent prediction period. (b) The predicted spatiotemporal evolution reconstructed from the three spatiotemporal patterns and their predicted principal components (PCs) in the independent prediction period. The ordinate is latitude and the abscissa is day of boreal summer in each year. (c) The prediction skills are assessed by the spatiotemporal pattern correlation between the predicted and observed spatiotemporal evolution only based on the three patterns in each boreal summer. The black vertical line separates the retrospective prediction skills in the training period of 1980–2009 from the independent prediction skills in the period of 2010–2022.

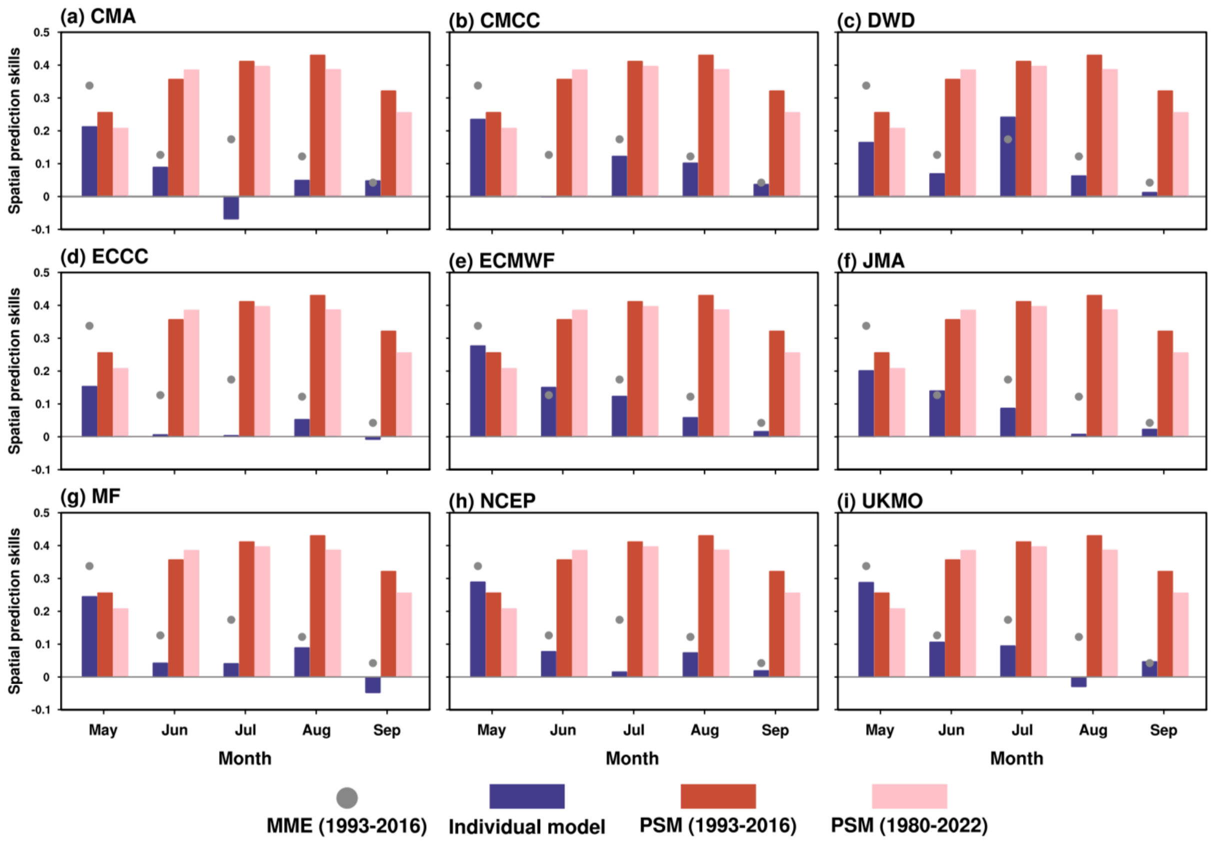

Supplementary Figure 7. Prediction skills for individual dynamical models. Multi-year mean forecast skills of the spatial pattern correlation against the total rainfall anomalies in individual months for each dynamical model and the physical-statistical prediction model (PSM). Grey dots indicate the multi-model ensemble (MME) mean forecast skill during 1993–2016 derived from nine dynamical models. The blue, red, and pink bars represent the prediction skills of the individual dynamical model (1993–2016), PSM (1993–2016), and PSM (1980–2022), respectively.

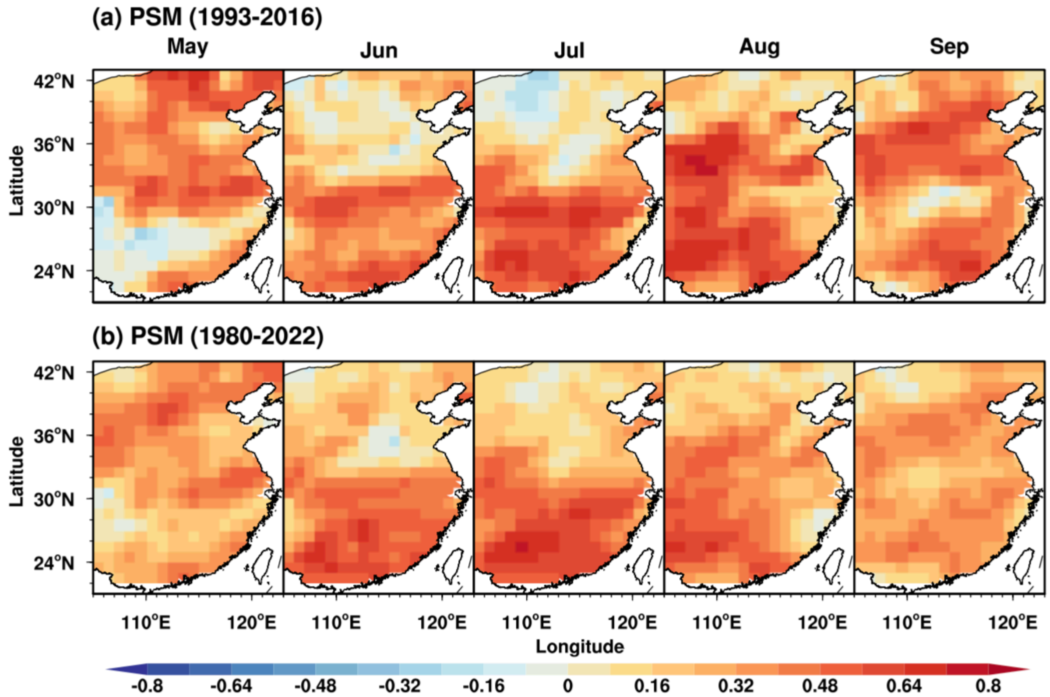

Supplementary Figure 8. Seasonal prediction skills for the spatiotemporal evolution of rainfall anomalies over East Asia. The forecast skills of temporal correlation against total observed anomalies of monthly and spatial rainfall anomalies in boreal summer using the physical-statistical prediction model (PSM) during (a)1993–2016 and (b) 1980–2022.

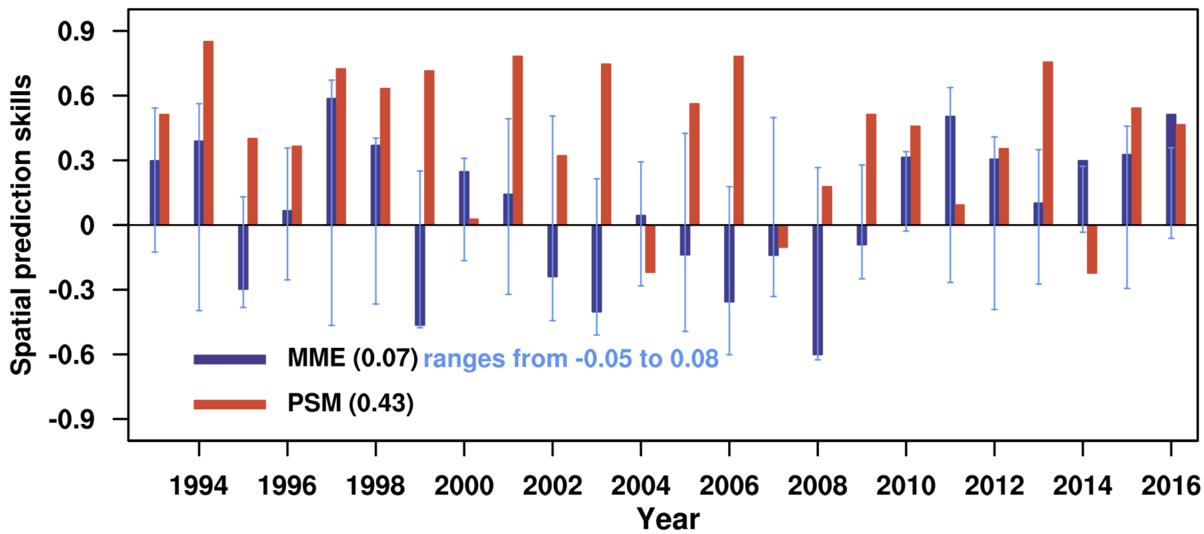

Supplementary Figure 9. Prediction skills of summer rainfall anomalies over continental East Asia. The prediction skills of spatial pattern correlation against the observed summer rainfall anomalies predicted by the multi-model ensemble (MME) mean of the dynamical models and the physical-statistical prediction model (PSM). The multi-year mean prediction skills during 1993–2016 for the MME and PSM are 0.07 and 0.43, respectively. The blue line segments represent the ranges of prediction skills derived from individual dynamical models.

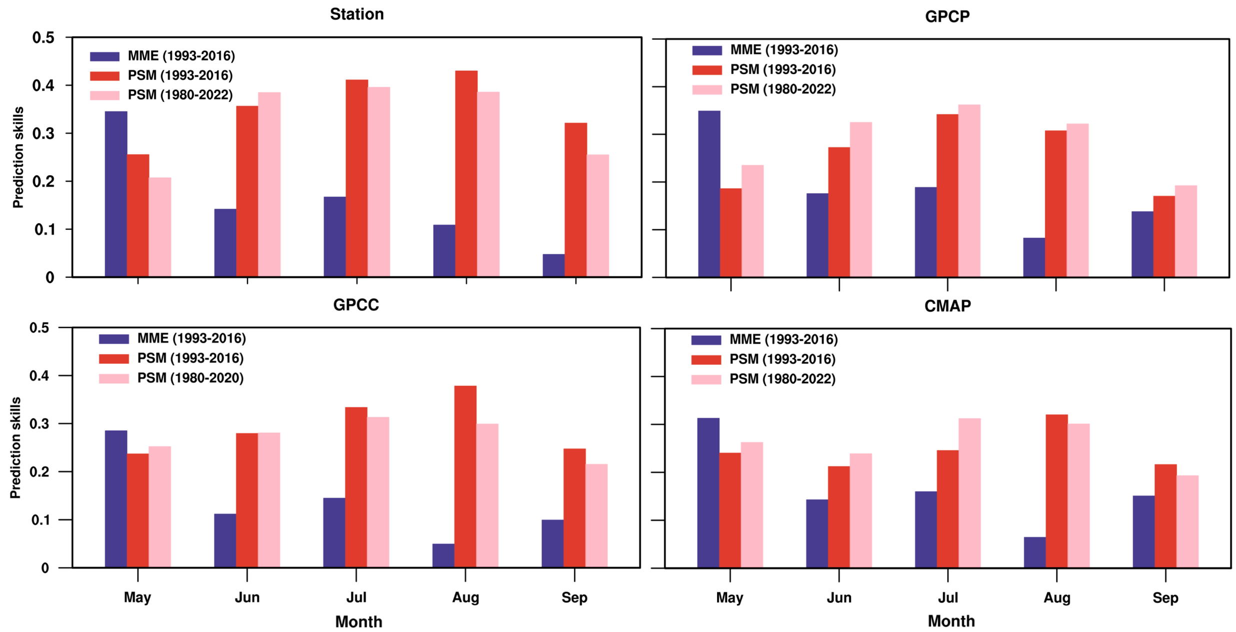

Supplementary Figure 10. Prediction skills against the observed spatiotemporal evolution of East-Asian rainfall anomalies in individual months. The multi-year mean forecast skills of the spatial pattern correlation against the total rainfall anomalies in each month during 1993–2016 in the multi-model ensemble (MME) mean of the dynamical models and the physical-statistical prediction model (PSM), based on different observation datasets. The abscissa represents the months of May through September.

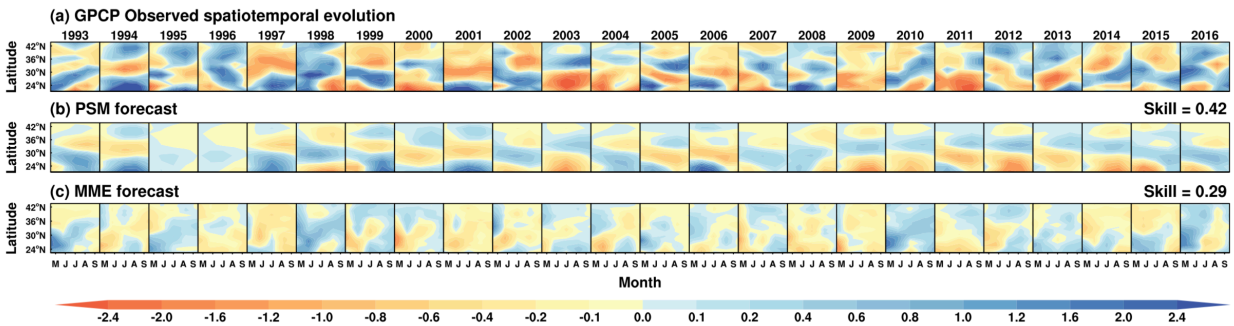

Supplementary Figure 11. Seasonal predictions against the observed spatiotemporal evolution of rainfall anomalies as function of latitude and month over East Asia. The spatiotemporal evolution is denoted by (a) the total rainfall anomalies derived from GPCP observation, (b) the predicted field from the physical-statistical prediction model (PSM), and (c) forecasted field from the multi-model ensemble (MME) mean of the dynamical models. The ordinate is latitude and the abscissa is month of boreal summer in each year. The overall forecast skills shown in the top right corner in (b) and (c) are assessed by the spatiotemporal correlation coefficient between forecasted and observed evolution of East-Asian rainfall anomalies for the period of 1993–2016.

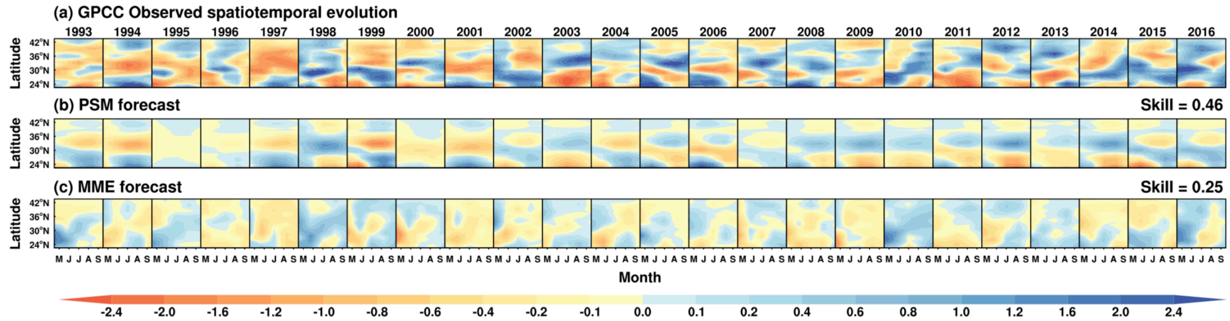

Supplementary Figure 12. Same as Supplementary Fig. 11, but for the GPCC.

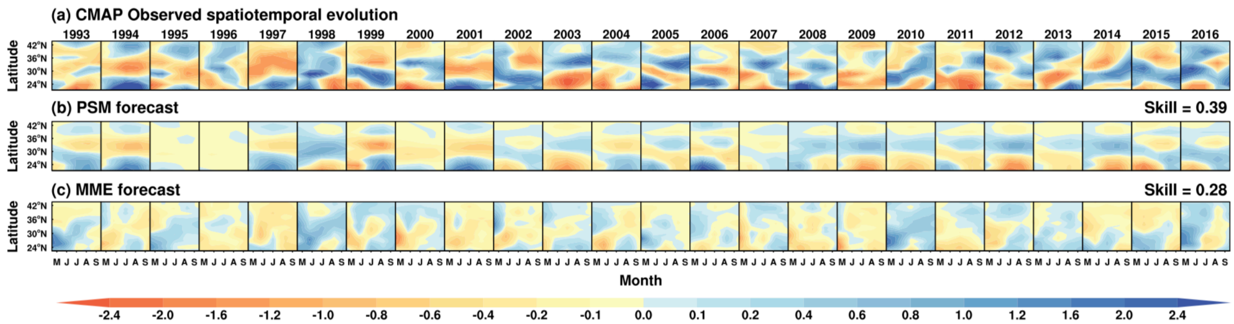

Supplementary Figure 13. Same as Supplementary Fig. 11, but for the CMAP.

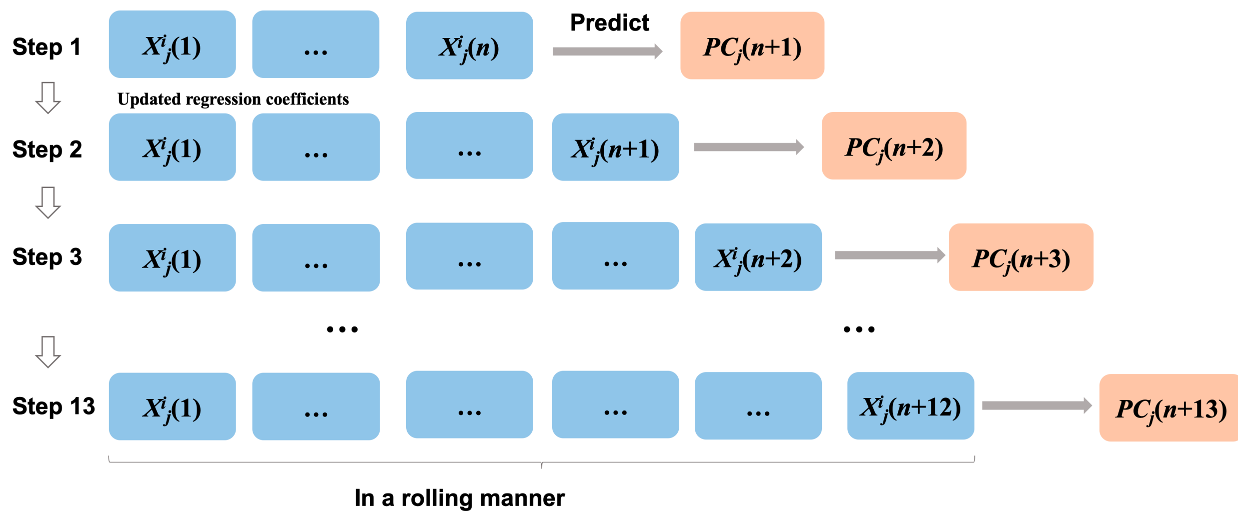

Supplementary Fig. 14. Schematic diagram of the independent retrospective prediction in a forward rolling manner. The independent prediction is based on the three multi-regression models derived from each PC_j (j = 1, 2, 3) and their two precursors (X^i_j, i = 1, 2).

Supplementary References

1. Ren, H.-L. et al. Prediction of primary climate variability modes at the Beijing Climate Center. *J. Meteor. Res.* **31**, 204–223 (2017).
2. Gualdi, S. et al. The new CMCC operational seasonal prediction system. Technical Note TN0288 (Centro Euro-Mediterraneo sui Cambiamennti Climatici, 2020).
3. Fröhlich, K. et al. The German climate forecast system: GCFS. *J. Adv. Model Earth Syst.* **13**, e2020MS002101 (2021).
4. Lin, H. et al. The Canadian Seasonal to Interannual Prediction System version 2.1 (CanSIPSv2.1). Technical Note. https://collaboration.cmc.ec.gc.ca/cmc/cmoi/product_guide/docs/tech_notes/technote_cansips-210_e.pdf (Environment and Climate Change Canada, 2021).
5. Johnson, S. J. et al. SEAS5: the new ECMWF seasonal forecast system. *Geosci. Model Dev.* **12**, 1087–1117 (2019).
6. Hirahara, S. et al. Japan Meteorological Agency/Meteorological Research Institute Coupled Prediction System version 3 (JMA/MRI-CPS3). *J. Meteor. Soc. Japan* **101**, 149–169 (2023).
7. Batté, L., Dorel, L., Ardilouze, C. & Guérémy, J.-F. Documentation of the Meteo-France seasonal forecasting system 8. http://www.umr-cnrm.fr/IMG/pdf/system8-technical.pdf (Meteo France, 2021)
8. Saha, S. et al. The NCEP climate forecast system version 2. *J. Clim.* **27**, 2185–2208 (2014).
9. MacLachlan, C. et al. Global Seasonal forecast system version 5 (GloSea5): A high-resolution seasonal forecast system. *Quart. J. Roy. Meteor. Soc.* **141**, 1072−1084 (2015).
10. Ma, J. R. et al. Pushing the boundary of seasonal prediction with the lever of varying annual cycles. *Sci. Bull.* **68**, 105–116 (2023).
11. Wu, R. G. & Kirtman B. P. Observed relationship of spring and summer East Asian rainfall with winter and spring Eurasian snow. *J. Clim.* **20**, 1285–1304 (2007).
12. Lee, S. S., Seo, Y. W., Ha, K. J. & Jhun, J. G. Impact of the western North Pacific subtropical high on the East Asian monsoon precipitation and the Indian Ocean precipitation in the boreal summertime. *Asia-Pac. J. Atmos. Sci.* **49**, 171–182 (2013).
13. Webster, P. J. & Yang, S. Monsoon and ENSO: Selectively interactive systems. *Q. J. R. Meteorol. Soc.* **118**, 877−926 (1992).
14. Adler, R. et al. The Global Precipitation Climatology Project (GPCP) monthly analysis (new version 2.3) and a review of 2017 global precipitation. *Atmosphere* **9**, 138 (2018).
15. Xie, P. & Arkin, P. Global precipitation: a 17-year monthly analysis based on gauge observations, satellite estimates, and numerical model outputs. *Bull. Amer. Meteor. Soc*. **78**, 2539–2558 (1997).
16. Schneider, U. et al. Evaluating the hydrological cycle over land using the newly-corrected precipitation climatology from the Global Precipitation Climatology Centre (GPCC). *Atmosphere* **8**, 52 (2017).